

Electro-Drop Bouncing in Low-Gravity

Erin S. Schmidt¹ and Mark M. Weislogel¹

Portland State University

(Dated: 20 November 2018)

We investigate the dynamics of spontaneous jumps of water drops from electrically charged superhydrophobic dielectric substrates during a sudden step reduction in gravity level. In the brief free-fall environment of a drop tower, with an external electric field drop dynamics are dominated by Coulombic force instead of gravity. These forces lead to a drop bouncing behavior similar to well-known terrestrial phenomena, though occurring for much larger drops (~ 0.5 mL). We provide a 1-dimensional model for the phenomenon, its scaling, and asymptotic estimates for drop time-of-flight in two regimes: at short-times close to the substrate when drop inertia balances Coulombic force due to net free charge and image charges in the dielectric substrate and at long-times far from the substrate when drop inertia balances free charge Coulombic force and drag. In both regimes the dimensionless electrostatic Euler number \mathbb{E}_u , which is a ratio of inertia to electrostatic force, appears as a key parameter.

I. SPONTANEOUS DROP JUMP

When a nonwetting, gravity-dominated sessile drop (e.g. a puddle) suddenly undergoes a large step reduction in Bond number it will spontaneously jump away from the surface. The Bond number is given by $\mathbb{B}_o \equiv \frac{\Delta\rho g R^2}{\gamma}$, where g is the acceleration, R is the characteristic interfacial length scale, $\Delta\rho$ is the difference in densities across the interface, and γ is the surface tension. The spontaneous drop jump was first observed experimentally in the Soviet Union by Kirk et al.¹ in 1970 for drops of mercury in hydrochloric acid, and later by Wollman et al. in 2016 for water drops in air². The motive force of the jump owes to the inertia of internal flows which occur as the interface deflects under the suddenly lessened \mathbb{B}_o . For drops with radial symmetry and sufficiently high initial \mathbb{B}_o , inward radial capillary waves constructively interfere at the axis, leading to geysering and creation of satellite droplets by the Rayleigh-Plateau breakup of the geyser. In the case of smaller jumping drops the capillary waves are quickly damped by viscous forces.

The physics of these relatively massive drops is far beyond the $1-g_0$ millimetric capillary length scale and tends to defy terrestrial expectations. However, such drops are also of critical practical importance to space systems design where examples of large capillary length scale multiphase flows are commonplace.

During the ‘roll-up’ of drops under ideal conditions, the spontaneous jump phenomenon is governed by a balance of inertia and surface tension forces, and once aloft the drop motion is nominally in a regime of pure drag. However, other forces can come into play.

In the course of our work with spontaneous drop jump we have occasionally observed jumped drops to decelerate and return to the superhydrophobic surface, rebounding multiple times in the fashion of rigid bodies bouncing under $1-g_0$. The forces at work in such situations are presumably electrostatic in origin. Examples of the phenomenon are shown as a time-lapsed composite image in Figure 1 for a 0.5 mL drop, and as a time-series in Figure 2 for a 0.05 mL drop.

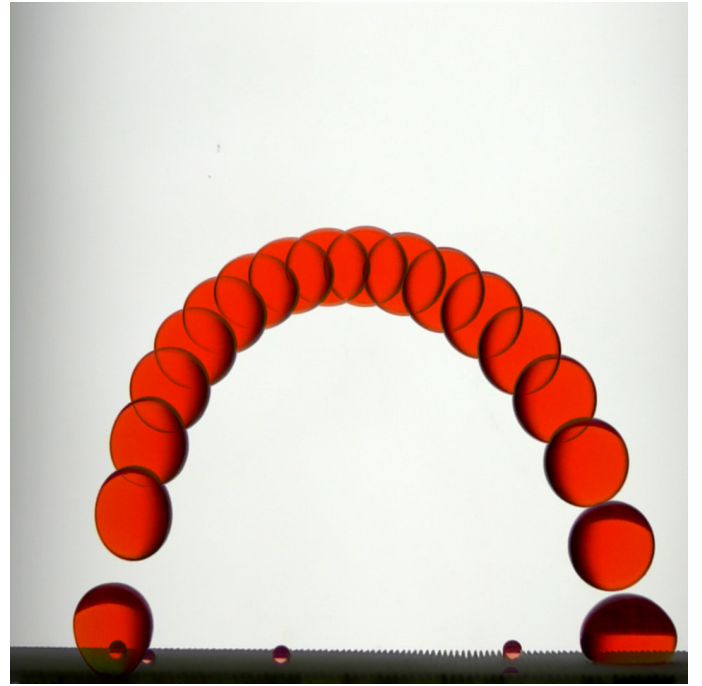


FIG. 1. The trajectory of a 0.5 mL drop is captured in a composite image over a single bounce period (~ 1.25 s) presented at ≈ 14 Hz. Motion of the drop is from left to right. The surface potential of the superhydrophobic dielectric is $\varphi_s = 1.25 \pm 0.41$ kV.

Preliminary observations of the phenomenon include:

- Observed maximum drop (de-)accelerations are on the order of ~ 30 cm/s² for a range of drop volumes $0.03 \lesssim V_d \lesssim 0.5$ mL.
- The water drops are attracted to regions of high electric field. The horizontal (surface plane parallel) components of the drop trajectory usually oscillate about some central position during the experiment, except in cases of nearly pure 1-D vertical translation. For especially small drops close to the spontaneous drop jump limit, identified by Attari

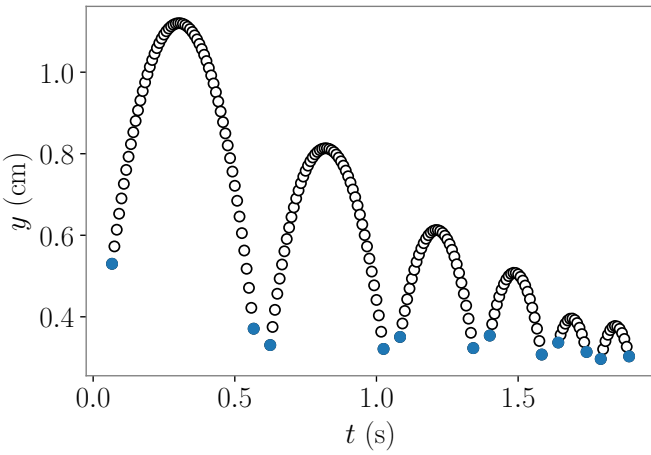


FIG. 2. The trajectory time-series of a 0.05 mL drop with surface potential $\varphi_s = 0.75 \pm 0.5$ kV.

*et al.*³ as $V_d \sim 0.01$ mL, the drops do not jump, but translate across the surface in a rolling regime until either a local maximum of the electric field is reached, or until their motion is sufficiently damped by contact line hysteresis that pinning arrests their motion.

- The drops appear to have net free charge. In cases of multiple simultaneous drop jumps the drops repel each other as they bounce or roll in orbital motion around regions of high field.
- The magnitude of the drop trajectory maxima (apoapses) are related to the drop volume (mass), and initial jump velocity (inertia), and to the electric field strength.

It is well known that water acquires positive free charge when in contact with certain polymers, especially polytetrafluoroethylene (PTFE), through a process called contact charging⁴. PTFE, on the other hand, tends to readily acquire negative charge by contact with water. The superhydrophobic surfaces used in the spontaneous drop jump experiments have thin (nanometric) PTFE coatings, and we observe that it is easy to produce significant surface potentials $\varphi_s \sim 100\text{-}500$ V by simply flowing streams of distilled water over them. A study of this water on PTFE contact charging phenomenon was conducted by Yatsuzuka *et al.*⁵, who suggest that this process results from formation of an electrical double layer driven by selective adsorption of (OH^-) ions at the polymer surface; other recent work supports this hypothesis^{6,7}. Given the large (roughness) ratio of projected to actual surface area of the superhydrophobic surfaces used in the experiment, and given that the drops are initially in a Cassie-Baxter state, a somewhat electrically resistive air layer is maintained that reduces grounding of the drops despite the large potential difference between them and the surface charges.

The source of the net free charge on the drops is another issue. The drop charge could be due to the contact charging mechanism mentioned previously. NASA flight engineer Don Pettit germanely discusses the problem of low-gravity flow induced charging of liquids resulting ultimately from contact charging phenomenon⁸. However, a more likely mechanism for the drop charge is field-induced charging occurring due to breakup of a conductor having a field-induced dipole (e.g., a physical separation of charge). In our work this might occur when a drop is deposited on the charged surface by a grounded syringe. The metal syringe needle tip and the liquid in the syringe itself are essentially a ground connection which is broken when the syringe is suddenly removed in the presence of an external electric field. Field-induced charging is at work in the famous Kelvin thunderstorm and is applied in inkjet and electrospray technologies, where in each case the breakup is by the Rayleigh-Plateau instability. Notably, in Pettit's aforementioned discussion of contact charging of liquids in low-gravity, he remarks on accidental electrostatic 'hula-ing' of silicone oil drops when ejected from a syringe in the vicinity of a highly-charged polymer surface during an experiment conducted aboard STS-5 by Space Shuttle mission specialist Joseph Allen⁸. Relatedly, in a series of informal and somewhat whimsical experiments Pettit himself electrostatically orbited small water drops around a triboelectrically charged PTFE knitting needle while aboard the International Space Station during expedition 30/31⁹. Again, in this case, the drop charge is likely field-induced.

The electro-drop bounce phenomenon may have useful applications in a space environment, generally to tackle various manifestations of the so-called "phase separation" problem of separating a gas phase from a multiphase flow (or the reverse case) in low-gravity. Removal of satellite droplets produced during pipetting in wet-lab research outside of a glovebox environment aboard the International Space Station has been recently suggested as an application of the work [private communication, NASA JSC, E. Unger, 2017]. Drops can become spontaneously charged by contact with standard micropipette tips¹⁰, and this free charge can be leveraged for the purposes of phase separation in low-gravity.

II. THEORY

A. Equation of Motion

We develop here a simple 1-dimensional model of the dynamics of drops dominated by electrostatic forces. We treat a drop as a particle with radius R_d , which translates vertically along the central axis of a charged dielectric square sheet substrate. The equation of motion for this system is given by,

$$my'' = -F_D - F_E, \quad (1)$$

subject to

$$y(0) = R_d, \quad \text{and} \quad y'(0) = U_0, \quad (2)$$

where m is the drop mass, $y'' = d^2y/dt^2$ is the drop acceleration, F_D is the drag force which always opposes motion, and F_E is the electrostatic force. The assumed initial conditions are such that, when Bo is suddenly reduced at the start of the drop tower free-fall period, the drop jumps with instantaneous initial velocity U_0 from its $1-g_0$ resting position of R_d at $t = 0$. The dynamical system is sketched schematically in Figure 3. We now define models for each of the forces in this equation.

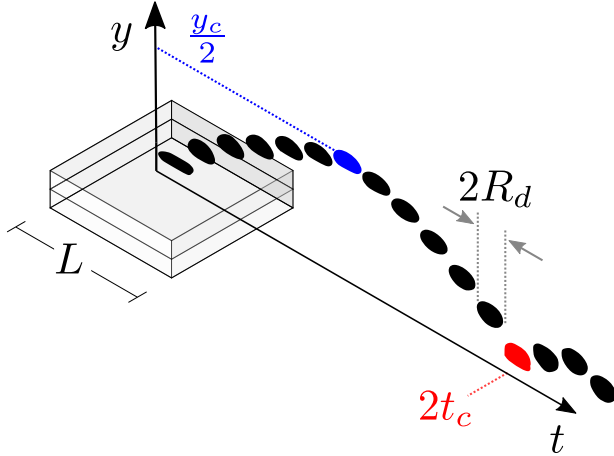


FIG. 3. Schematic representation of drop jump with return and rebound from an electrically charged superhydrophobic substrate. The characteristic time and length scales t_c and y_c describe the time of flight and apoapse associated with the drop trajectory. L denotes the length scale characteristic of the charged superhydrophobic substrate.

For the intermediate range of Reynolds numbers $1 \leq \text{Re} \equiv \frac{2UR_d}{\nu} \leq 50$ observed in our experiments, we assume the force of drag acting on the drop to be quadratic, with ν being the kinematic viscosity.

In modeling the electrostatic force we begin with the standard electrohydrodynamic (EHD) approximation¹¹. Supposing that electrical forces acting on free charges and dipoles in a fluid are transferred directly to the fluid itself, the overall electrical body force density will be the divergence of the Maxwell stress tensor τ_m ,

$$\begin{aligned} \mathbf{F}_E &= \nabla \cdot \tau_m \\ &= \rho_f \mathbf{E} + \frac{1}{2} |E|^2 \nabla \epsilon - \nabla \left(\frac{1}{2} \rho \left(\frac{\partial \epsilon}{\partial \rho} \right)_T |E|^2 \right). \end{aligned} \quad (3)$$

The first term on the right hand side of this expression is the well known Coulombic force or electrophoretic force, which arises from the presence of free charge in an external electric field. We expect this term to dominate the electric force in a DC field. The second term is the force arising from polarization stresses due to a nonuniform field acting across a gradient in permittivity. This force is widely termed the dielectrophoretic (DEP) force.

The third term describes forces due to electrostriction. It has been noted by Melcher and Hurwitz¹² that the electrostriction term is the gradient of a scalar and can thus be canonically lumped together with the hydrostatic pressure for incompressible fluids. We neglect it in our analysis.

It is common to approximate the dielectrophoretic force by idealizing the drop as a simple dipole using the effective dipole moment method first described by Pohl in 1958¹³. The force felt by the dipole is

$$\begin{aligned} \mathbf{F}_{DEP} &= (\mathbf{P}_e \cdot \nabla) \mathbf{E} \\ &= 2\pi R_d^3 \kappa_w \epsilon_0 K \nabla E^2, \end{aligned} \quad (4)$$

where $\mathbf{P}_e = (\kappa_w - \kappa_a) \epsilon_0 \mathbf{E}$ is the excess polarization, ϵ_0 is the vacuum permittivity, and κ_w and κ_a are the relative dielectric constants of the water particle and air host fluid, respectively. Here it is convenient to use the simplifying shorthand $K = \frac{\kappa_w - \kappa_a}{\kappa_w + 2\kappa_a}$, known as the Clausius-Mossotti factor. In cases where $K < 0$, or $K > 0$ the particle will be respectively repelled or attracted to regions of strong field. By comparing DEP and Coulombic forces we note that a condition to neglect the DEP force is

$$\frac{\kappa_w \epsilon_0 K R_d^2 E_0}{q} \ll 1.$$

This condition prevails in our experiments and we henceforth neglect the DEP force.

When the drop is close to the dielectric surface, the free charge on the drop will tend to induce polarization of the dielectric which perturbs the electric field. The polarization bound charge in the dielectric will be of the opposite sign of the free drop charge and thus there will be a force of attraction. This so-called image force is a correction to the Coulomb force due to the external electric field only, and can be found by a Green's Function solution of Laplace's equation for the electric field, the so-called 'method of images'¹⁴. This resulting image force \mathbf{F}_I is given by

$$\mathbf{F}_I = \frac{kq^2}{16\pi\epsilon_0} y^{-2} \hat{\mathbf{j}}, \quad (5)$$

where the factor k is a function of the dielectric surface susceptibility $k = \frac{\chi_e}{\chi_e + 2}$, $\chi_e = \kappa_d - 1$, κ_d is the relative dielectric constant of the dielectric substrate, and $\hat{\mathbf{j}}$ is a unit vector normal to the dielectric surface.

By substituting Equation 5 into 3 we have for a single drop

$$\begin{aligned} \mathbf{F}_E &= q\mathbf{E} + \mathbf{F}_I \\ &= q\mathbf{E} + \frac{kq^2}{16\pi\epsilon_0} y^{-2} \hat{\mathbf{j}} \end{aligned} \quad (6)$$

Thus the 1-D governing Equation 1, becomes

$$my'' = -\frac{1}{2} C_D \rho A y'^2 - qE - \frac{kq^2}{16\pi\epsilon_0} y^{-2}, \quad (7)$$

subject to

$$y(0) = R_d, \quad \text{and} \quad y'(0) = U_0. \quad (8)$$

B. Electric Field

If we consider the charged dielectric surface of our experiments to be a square sheet of charge lying in the xz -plane with width L , the symmetry of the problem happily lets us obtain the y -component of the electric field \mathbf{E} by direct integration (as a superposition of line charges)¹⁴ as

$$E = \frac{\sigma}{\pi\epsilon_0} \tan^{-1} \left(\frac{L^2}{y\sqrt{2L^2 + 4y^2}} \right), \quad (9)$$

where σ is the surface charge density. We note that this 1D model of the electric field is valid when $R_d \ll L$, which will be true for cases of small drops ‘far’ from the dielectric surface.

By taking Taylor series expansions in large and small y -limits we gain some insight about the behavior of this field. In the limit $y/L \ll 1$ Equation 9 reduces to

$$E \approx \frac{\sigma}{4\pi\epsilon_0} = E_0, \quad (10)$$

where E_0 is the characteristic electric field. This field is constant and equivalent to the electric field due to an infinite plane of charge. In the limit of $y/L \gg 1$, Equation 9 reduces to the familiar electric field due to a point charge

$$E \approx L^2 E_0 y^{-2}. \quad (11)$$

Equation 9 with both regimes given by 10 and 11 are identified in Figure 4.

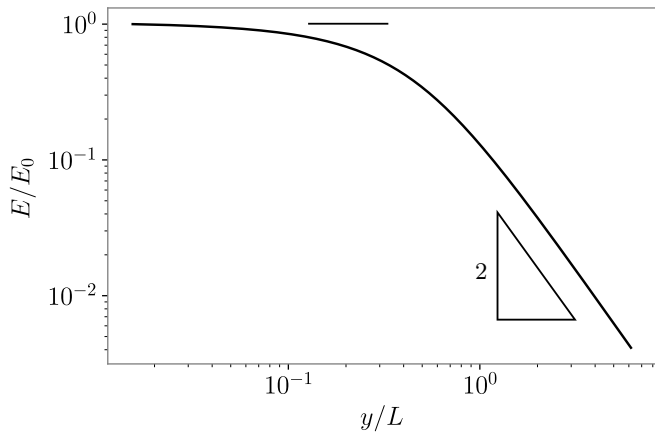


FIG. 4. A log-log plot of the magnitude of the dimensionless electric field E .

C. Scaling

Equation 7 is non-linear, non-homogeneous and must be solved numerically. Nevertheless we seek approximate

solutions to the equation analytically using perturbation methods. Introducing the scaled variables

$$t^* = \frac{t}{t_c}, \quad y^* = \frac{y}{y_c}, \quad (12)$$

where y_c and t_c are characteristic length and time scales, and using the coordinate transformation $y(0) - R = 0$, the governing Equation 7 becomes

$$y^{*''} = -\Pi_1 y^{*'^2} - \Pi_2 E^*(y^*) - \Pi_3 (\Pi_4 y^* + 1)^{-2}, \quad (13)$$

subject to

$$y^*(0) = 0, \quad \text{and} \quad y^{*'}(0) = \Pi_5,$$

where we note the existence of several dimensionless groups

$$\begin{aligned} \Pi_1 &= \frac{C_D \rho A y_c}{2m}, & \Pi_2 &= \frac{q E_0 t_c^2}{m y_c}, & \Pi_3 &= \frac{k q^2 t_c^2}{16 \pi \epsilon_0 R_d^2 m y_c}, \\ \Pi_4 &= \frac{y_c}{R_d}, & \Pi_5 &= \frac{U_0 t_c}{y_c}. \end{aligned}$$

1. Inertial Electro-Image Limit

In the limit of small y and t we expect inertia to scale with Coulombic and image forces. In this limit we can approximate the electric field as the constant E_0 . One possible characteristic length scale is $y_c \sim R_d$, however this scale is overly restrictive with respect to time. With $y_c \sim U_0 t_c$ and picking t_c such that the Coulombic force $\Pi_3 \sim \mathcal{O}(1)$, the intrinsic scales are found such that

$$t_c \sim \frac{m U_0}{q E_0}, \quad \text{and} \quad y_c \sim \frac{m U_0^2}{q E_0}.$$

With these scales Equation 13 becomes

$$y^{*''} = -1 - \mathbb{I}g (\mathbb{E} u y^* + 1)^{-2}, \quad (14)$$

subject to

$$y^*(0) = 0, \quad \text{and} \quad y^{*'}(0) = 1.$$

with

$$\mathbb{I}g \equiv \frac{kq}{16\pi\epsilon_0 R_d^2 E_0} = \Pi_3, \quad \mathbb{E}u \equiv \frac{m U_0^2}{q E_0 R_d} = \Pi_4,$$

where the Image number $\mathbb{I}g$ is the ratio of image forces to the Coulombic force of the unperturbed field, and the electrostatic Euler number $\mathbb{E}u$ is the ratio of inertia to electrostatic force, or equivalently, in a conservative system $\mathbb{E}u$ can be thought of as a ratio of kinetic energy $m U_0^2$ and electrostatic potential energy $q E_0 R_d$.

2. Inertial Electro-Viscous Limit

In the limit of large y and t we expect drop inertia to balance Coulombic force and drag. Here we approximate the electric field as $E \approx y_c^2 E_0 y^{-2}$. We choose the scaling $y_c \sim U_0 t_c$ and $\Pi_3 \sim \mathcal{O}(1)$ for its combination of physical simplicity, few Π terms, and homogeneous initial conditions. The intrinsic scales for this case are given by

$$t_c \sim \frac{R_d^2}{L^2} \frac{4\pi m U_0}{q E_0} \quad \text{and} \quad y_c \sim \frac{R_d^2}{L^2} \frac{4\pi m U_0^2}{q E_0}.$$

With these scales Equation 13 becomes

$$y^{*''} = -\mathbb{D}g \mathbb{E}u y^{*'^2} - (\phi \mathbb{E}u y^* + 1)^{-2}, \quad (15)$$

subject to

$$y^*(0) = 0, \quad \text{and} \quad y^{*'}(0) = 1,$$

where we call $\mathbb{D}g$ the drag number $\mathbb{D}g \equiv \frac{C_D \rho_a}{\rho_l} = \Pi_1 \phi^{-1} \mathbb{E}u^{-1}$, and $\phi = 4\pi \frac{R_d^2}{L^2}$ is a drop-to-substrate aspect ratio.

D. Asymptotic Estimates

Equations 14 and 15 are weakly non-linear differential equations in the sense that they reduce to linear equations as $\mathbb{E}u \rightarrow 0$. For $\mathbb{E}u \ll 1$ we find asymptotic solutions of the non-linear equations by means of regular perturbations. In this case we use the naive expansion

$$y^*(t^*) \sim y_0^*(t^*) + \mathbb{E}u y_1^*(t^*) + \mathbb{E}u^2 y_2^*(t^*) \dots \mathbb{E}u^n y_n^*(t^*). \quad (16)$$

1. Inertial Electro-Image Limit

Substituting Equation 16 and its derivatives into 13, and equating terms by order we find the $\mathcal{O}(1)$ unperurbed solution

$$y_0^*(t^*) = t^* + \frac{t^{*2}}{2} (-1 - \mathbb{I}g).$$

By inspection, it is evident that if $\mathbb{I}g = 0$, the solution is the classical kinematic equation for projectile motion without drag under constant gravity g_0 . Continuing on to higher order, after some tedious computations documented in the project repository for this work¹⁵, we find the $\mathcal{O}(\mathbb{E}u^5)$ order accurate solution which is truncated to $\mathcal{O}(\mathbb{E}u^2)$ below:

$$y^*(t^*) = t^* + \frac{t^{*2}}{2} (-1 - \mathbb{I}g) + \mathbb{E}u \left(\frac{\mathbb{I}gt^{*3}}{3} + \frac{\mathbb{I}gt^{*4}}{12} (-1 - \mathbb{I}g) \right) + \mathcal{O}(\mathbb{E}u^2). \quad (17)$$

We plot the approximate short-time solution of Equation 17 with varying values of $\mathbb{I}g$ in Figure 5. These plots show a trend of decreasing time-of-flight t_f , which is the time for the drop to return to the origin (a single ‘bounce’), and height at apoapse with increasing values of $\mathbb{I}g$. Trajectories with $\mathbb{E}u \leq 0.1$ are essentially coincident given the scale of the axes used here. In principle there is some coupling between $\mathbb{E}u$ and $\mathbb{I}g$; notably this relationship does not depend on the electric field E_0 but on a charge to mass ratio. The effect of contact line hysteresis on the initial jump velocity U_0 will also tend to decohere the natural covariance between these parameters.

2. Inertial Electro-Viscous Limit

By similar arguments we find an asymptotic estimate of the trajectory in the long-time regime. If we assume a constant scale for the drag coefficient $C_D \approx 0.5$ then $\mathbb{D}g$ is approximately a constant $\mathbb{D}g \approx 6 \times 10^{-4}$ in all of our experiments. The approximate solution is

$$\begin{aligned} y^*(t^*) &= t^* - \frac{t^{*2}}{2} \\ &+ \phi \mathbb{E}u \left(\frac{t^{*3}}{3} (1 + \mathbb{D}g) + \frac{t^{*4}}{12} (-1 - \mathbb{D}g) - \frac{\mathbb{D}gt^{*2}}{2} \right) \\ &+ \mathcal{O}(\phi^2 \mathbb{E}u^2). \end{aligned} \quad (18)$$

Trajectories for this solution are shown in Figure 6. We note that the trajectory reduces to the classical $\mathcal{O}(1)$ solution for small values of $\phi \mathbb{E}u$. We also note that with $\mathbb{D}g = 6 \times 10^{-4}$ the effect of drag is slight, appearing only as a slight correction to the higher order terms.

By again applying a regular perturbation to the asymptotic solution, Equation 18, with the expansion

$$t^* \sim t_0^* + \phi \mathbb{E}u t_1^* + \phi^2 \mathbb{E}u^2 t_2^* \dots \phi^n \mathbb{E}u^n t_n^*,$$

and solving for the roots at times when $y^* = 0$, we find an asymptotic estimate for the time-of-flight. The $\mathcal{O}(\phi^2 \mathbb{E}u^2)$ accurate time-of-flight estimate is given by

$$\begin{aligned} t_f &= 2 + \phi \mathbb{E}u \left(\frac{4}{3} - \frac{2\mathbb{D}g}{3} \right) + \phi^2 \mathbb{E}u^2 \left(\frac{4}{5} - \frac{4\mathbb{D}g}{3} + \frac{2\mathbb{D}g^2}{5} \right) \\ &\quad + \mathcal{O}(\phi^3 \mathbb{E}u^3). \end{aligned}$$

Substituting the experimental value of $\mathbb{D}g$ we find the time-of-flight estimate for water drops is

$$t_f = 2 + 1.333\phi \mathbb{E}u + 0.799\phi^2 \mathbb{E}u^2 + \mathcal{O}(\phi^3 \mathbb{E}u^3). \quad (19)$$

As $\phi \mathbb{E}u$ grows to be no longer small, the time-of-flight grows rapidly with an asymptote at a certain critical velocity; this is an electrostatic escape velocity U_e . We can find the escape velocity by solving a limiting version of the equation of motion

$$mu' = -\frac{qE_0 y_c^2}{y^2},$$

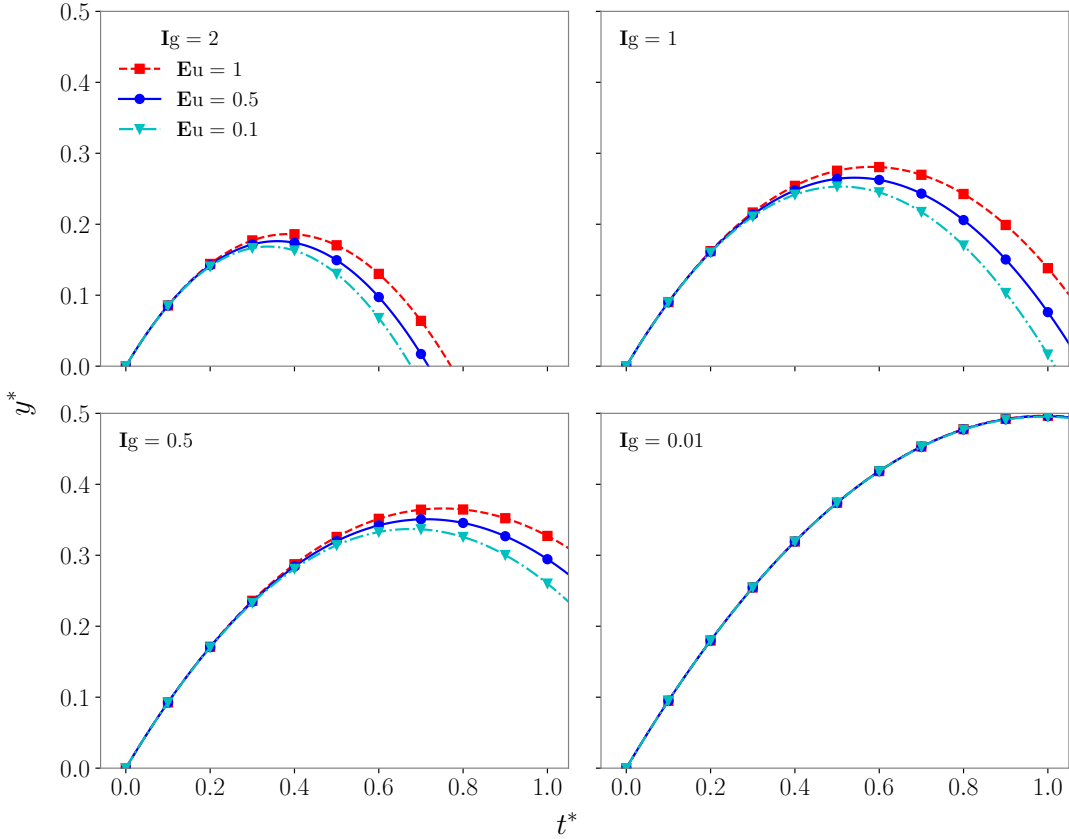


FIG. 5. Short-time scaled drop trajectories for various values of $\mathbb{E}u$, $\mathbb{I}g$. The trajectory reduces to the classical $\mathcal{O}(1)$ solution for small values of $\mathbb{I}g$. It should be noted that despite what is implied by these plots $\mathbb{I}g$ is not necessarily independent of $\mathbb{E}u$, sharing q and E_0 as common factors, as well as the covariance relationships $U_0 \propto R_d^2$, and $m \propto R_d^3$.

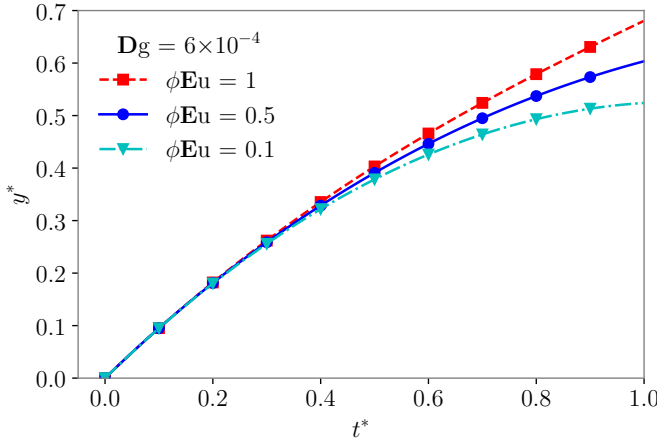


FIG. 6. Long-time scaled drop trajectories for various values of $\phi\mathbb{E}u$.

where $u = \frac{dy}{dt}$ is the drop velocity. This has the solution

$$u(y) = \pm U_0 \left(1 + \frac{2qE_0y_c^2}{mU_0^2} \left(\frac{1}{y} - \frac{1}{R_d} \right) \right)^{1/2}.$$

This equation has an asymptotic velocity U_∞ at $y = \infty$, which is real provided

$$U_0 \geq U_e = y_c \sqrt{\frac{2qE_0}{mR_d}},$$

where U_e is the escape velocity and $U_\infty = \sqrt{U_0^2 - U_e^2}$. If $y_c = L$ the condition for the drops to escape the electric field is then given by

$$\frac{1}{8\pi}\phi\mathbb{E}u > 1. \quad (20)$$

III. METHODS

A. Overview

Using various scaling arguments we have gleaned from our simple model a set of dimensionless numbers characteristic of drop bounce apoapses and times of flight. The dimensionless numbers depend on physical properties not all of which are easily measured by experiment. In particular, direct determination of net drop free electric charge q is difficult as high-input resistance electrometers are not

well-suited to the sudden $15-g_0$ decelerations characteristic of drop tower experiments. To estimate the drop free charge q we use parameter estimation techniques. Our work flow to identify q in a drop tower experiment is as follows:

1. We vary the independent variables drop volume V_d and dielectric surface charge density σ in a set of single-drop spontaneous drop jump experiments under low-gravity in a 2.1 s drop tower.
2. We capture video and digitize the trajectories of the drops.
3. We solve the inverse problem to find the drop free charge q by maximizing the log-likelihood of the experimental trajectories given the dynamical model by varying the parameter vector $\mathbf{x} = \langle q, V_d, \sigma \rangle$ using a direct search optimization.

B. Experimental Methods

The Dryden Drop Tower at Portland State University uses a dual capsule design, inspired by the 2.2 s facility at NASA Glenn Research Center, which decouples drag acceleration felt by the external drag shield from the experiment. The experiment experiences approximately $\lesssim 1 \times 10^{-4} g_0$ during free-fall for 2.1 s as the experiment and drag shield plummet together to the bottom of the tower 6 stories below. A drop tower rig with a mounted experiment is shown in Figure 7. Single drops of distilled water in a range of volumes ($0.01 \leq V_d \leq 0.5 \text{ mL}$) are carefully deposited on rig-mounted charged superhydrophobic substrates using a grounded glass syringe with $\pm 1 \mu\text{L}$ accuracy and then dropped in the drop tower. In this work 16 such single-drop drop jump experiments are conducted. Drops are colored with red dye to improve thresholding accuracy in trajectory digitization. Drop trajectories are captured using a Panasonic HC-WX970 Camera recording at 120 fps. Drop trajectories are digitized from the video recordings using the particle tracking module in Fiji¹⁶.

Superhydrophobic electret substrates are prepared with surface potentials $\varphi_s = 0.4\text{-}1.8 \text{ kV}$. We use an isothermal electret formation process which is a variation of the widely applied corona-charging technique. A Ptec IN5120 balanced AC corona ion source directs a net neutral stream of ions towards a dielectric substrate, which we polarize by an embedded electrode with an EMCOP20P 2 kV+ absolute reference DC-DC converter. The ion stream compensates the surface and space bound charges arising due to the polarization of the dielectric. After the corona source and DC-DC converter are powered off and the electrode is shorted across a bleed resistor, the deposited negative ions remain on the substrate surface. The electret is lamina of 3 to 4 0.4 mm thick corona charged polymethyl methacrylate (PMMA) sheets. The electric field strength scales with the number

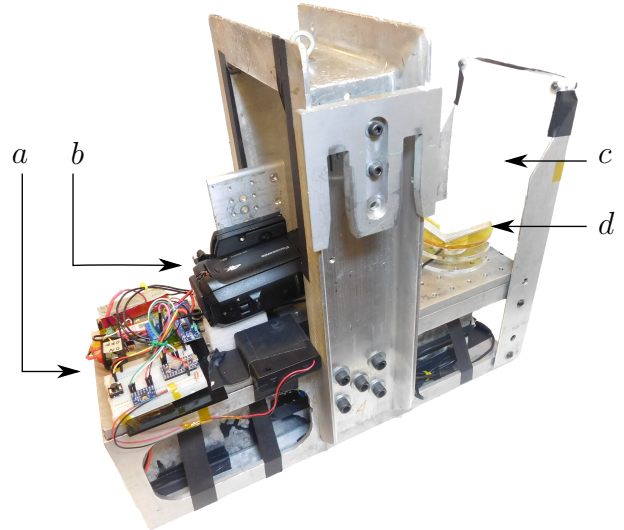


FIG. 7. The electro-drop bounce experiment hardware mounted on a drop tower rig. (a) HV DC-DC converter and control electronics. (b) Camera. (c) Light panel. (d) Test cell.

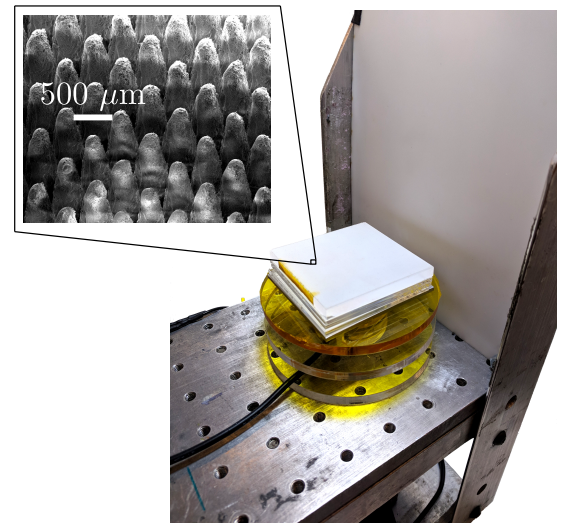


FIG. 8. Close up of the experimental test cell.

of dielectric lamina as has also been shown in work on laminated electret based vibrational energy harvesters¹⁷ and in water desalinating¹⁸. The RC time constant for decay of the surface charge is observed to be $\tau \approx 2000 \text{ s}$.

The topmost face of the electret lamina is made superhydrophobic by first laser ablating a pillar topology on the surface followed by deposition of a thin layer of PTFE. We use a pattern with pillar heights $\sim 775 \mu\text{m}$, widths $\sim 70 \mu\text{m}$, and pitch $\sim 100 \mu\text{m}$. An SEM image of the pillar geometry is shown in Figure 8. Contact angles of distilled water on the surface, measured using the tangent method, are $\approx 150^\circ$ when the surface is uncharged. The roll-off angle of a 1 mL drop is $1^\circ \pm 0.5^\circ$.

Surface potentials φ_s are measured on the superhy-

drophobic surface using a Simco-Ion FMX-004 electrostatic fieldmeter and the method for determination of surface charge density for low conductivity polymers described in Davies¹⁹. For this measurement the fieldmeter is shielded, the electret substrate rests over a conductive ground plane, and the surface charge density is determined from $\sigma = \varphi_s \kappa \epsilon_0 / l$, where l is the thickness of the dielectric substrate. The relative dielectric constant of the PMMA sheet κ , is measured by using a 65×65 mm polished aluminum parallel plate capacitor with $C = \kappa \epsilon_0 A / l$, where C is the capacitance, and A is the sheet area. Measuring the capacitance with 3 sample thicknesses using a GenRad 1657 RLC Dibridge, we find the relative permittivity to be $\kappa = 3.5 \pm 0.4$.

C. Parameter Estimation

We generally seek the parameters \mathbf{x} that solve the inverse problem $G(\mathbf{x}) + \mathbf{u} = \mathbf{d}$, where the model $G(\mathbf{x})$ describes some relationship between the vector of parameters \mathbf{x} and a set of observations \mathbf{d} , and where \mathbf{u} is the measurement error. In particular we seek the parameter set $\mathbf{x} = \langle q, V_d, \sigma \rangle$ that has the highest probability (i.e. the maximum of the posterior Probability Density Function) of observing the data given the model, which is a numerical solution to Equation 7. This can be determined by maximizing the log-likelihood (or equivalently by minimizing χ^2 goodness-of-fit) of the data \mathbf{d} with respect to the model. This problem is formally stated as

$$\min \chi^2 = \min \sum_{i=1}^n \frac{(y_d(t)_i - y_G(t, \mathbf{x})_i)^2}{\sigma_{di}},$$

$$\mathbf{x} = \begin{cases} q \\ V_d \\ \sigma \end{cases}, \text{ subject to constraints } g = \begin{cases} V_d \pm u_{exp} \\ \sigma \pm u_{exp} \\ y_0 \pm u_{exp} \\ t_0 \pm u_{exp} \end{cases},$$

where $y_G(t, \mathbf{x})$ is the y -coordinate position at time t of the numerical solution of the equation of motion, $y_d(t)$ is the corresponding experimentally observed drop y -coordinate position at time t , σ_d is the standard error of the observed position, and u_{exp} are the measurement uncertainties. The vector \mathbf{x} that minimizes χ^2 is the so called Maximum Likelihood Estimate (MLE) of the experimental parameters.

We integrate Equation 7 numerically using the *netlib ODEPACK lsoda* integrator implemented as `scipy.integrate.odeint` in the *Scipy*²⁰ library in Python. The optimization problem in this case is non-convex, mixed discrete-continuous black-box (noisy), and highly ill-conditioned. The ill-conditioning arises due to the strong covariance between several of the model parameters, namely $q = q(V_d, E_0)$. The non-convexity of the problem implies that there are many local minima of the objective function. To solve the optimization problem we employ the gradient-free

direct-search Nelder-Mead²¹ algorithm implemented as `scipy.optimize.minimize(method='Nelder-Mead')` in *SciPy*. Nelder-Mead is relatively robust to noise and is thrifty with our computationally expensive function-calls. Experimental trajectory data is smoothed using a Savitsky-Golay filter²² to improve the convergence characteristics of the optimizer. This filter is implemented as `scipy.signal.savgol_filter` in *SciPy*. We precondition the optimization problem by minimizing $\ln(\chi^2)$ and using a naive $\sim \mathcal{O}(1)$ scaling of our constraints by their initial guesses. Here the goal is to make the problem equally sensitive to steps in any direction. The so-called identifiability problem of bounding uncertainty of the parameter estimates is resolved by constraining the parameter values by our experimental observations of them and their associated measurement uncertainties. Because Nelder-Mead cannot be used for explicitly constrained problems we implement the constraints using an exterior penalty function.

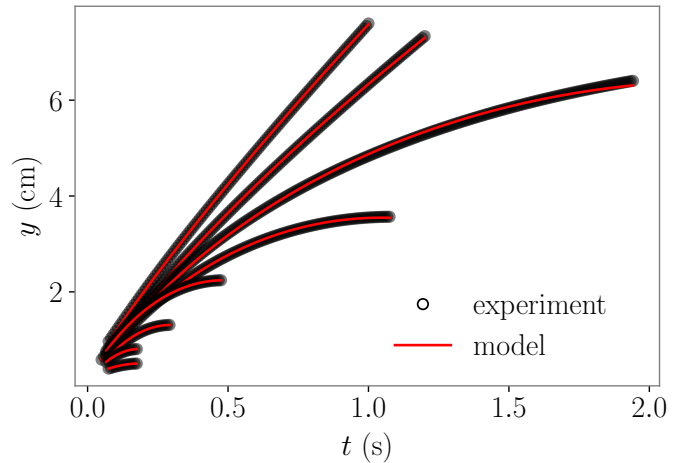


FIG. 9. A set of drop trajectories showing the results of the parameter estimation. The trajectories are shown only up to the first apoapse before rebound. The (—) lines show the numerical solution of Equation 7 with the given MLE parameter vector. χ^2 goodness-of-fit varies between 1×10^{-5} and 1×10^{-8} with the better fit occurring typically for the drops with the lowest apoapses.

IV. RESULTS

A. Parameter Estimates

The MLE estimates of q , as well as the measured values of V_d , E_0 , and U_0 for the entire population of drop tower tests are shown in the scatter plot matrix of Figure 10. The dependence of charge on drop volume V_d is immediately evident, while the effect of electric field on drop charge is less obvious. This co-linearity is the source of the ill-conditioning in the parameter estimation process.

However, assuming the main effect is the interaction between charge and electric field, a forced entry Robust Least Squares model

$$q \sim kAE_0, \quad (21)$$

with the transformation $A = V_d^{2/3}$ finds that $k = 7.589 \times 10^{-11} \pm 1.47 \times 10^{-11}$ F/m with $R^2 = 0.65$ and $F = 27$.

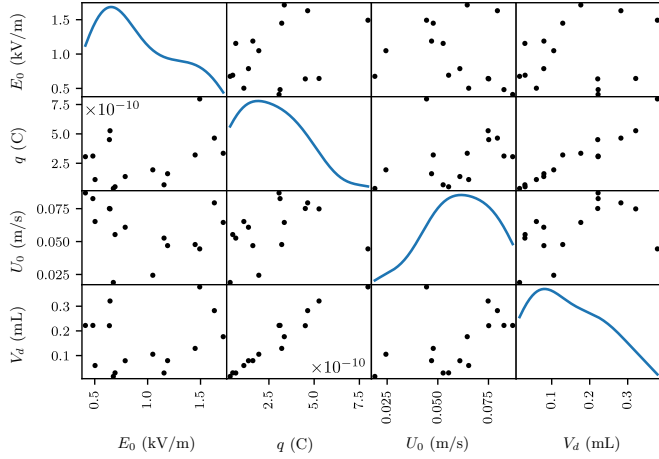


FIG. 10. Scatter plot matrix of main parameters E_0 , U_0 , V_d , and q .

A two-way T-test comparison of charge distributions between the drop bounce experiment and a corollary experiment with zero electric field at the time of drop deposition on the superhydrophobic surface suggests that the drop charge is primarily induced by the electric field, rather than developed through contact charging on the PTFE layer ($t = 5.11$, $p = 0.0002$).

Incidentally, the model $q \sim kAE_0$ is similar to the classical solution for the surface charge of a half-spherical conductor with a field-induced dipole¹⁴

$$\begin{aligned} q &= 3\epsilon_0 E_0 \int_A \cos \theta dA \\ &= 3\pi^{1/3} 6 (6V_d)^{2/3} \epsilon_0 E_0 \int_0^{\pi/2} \cos \theta d\theta \\ &= kAE_0 \end{aligned} \quad (22)$$

with $k \approx 1.3 \times 10^{-10}$ F/m. This is also of similar form to the charge found experimentally by Takamatsu and coauthors for drops falling from a grounded nozzle in an external electric field²³

$$q = 4\pi\epsilon_0\beta E_0 R_d^2 \quad (23)$$

with $\beta \approx 2.63$. Casting Equation 23 in the same form as Equations 21 and 22, $k \approx 4\pi\epsilon_0\beta(4\pi/3)^{-2/3} \approx 1.1 \times 10^{-10}$ F/m.

The effect of volume on jump velocity U_0 is not immediately evident in the data despite previous work having establishing this relationship³. This likely results from

large variance in U_0 due to contact line hysteresis during the drop roll-up. Contact line losses predominate in the < 1 mL volume drops which are primarily the object of this study.

B. Model Validation

Using the parameter estimates we find $\mathbb{E}u$ for each drop jump. Dimensional drop apoapses shown in Figure 11 scale with $\mathbb{E}u$ as expected according to our earlier analysis. Electrostatic Euler numbers in the data set vary between $1.4 \lesssim \mathbb{E}u \lesssim 35.4$. In the non-dimensional trajectories with short-time scaling shown in Figure 12, we see that the scaled trajectory apoapses are consistently $\mathcal{O}(1)$, with all trajectories overshooting their characteristic time scale (which predicts returns at $t^* = 2$ at zeroth order). A trend of increasing $\max(y^*)$ at apogee for decreasing $\mathbb{E}u$ is seen in Figure 13. This trend seems to decay to a constant $y_{max}/y_c \approx 1/2$ for $6 \lesssim \mathbb{E}u \lesssim 20$, and implies the existence an intermediate regime with a larger characteristic lengthscale for $\mathbb{E}u \gtrsim 6$.

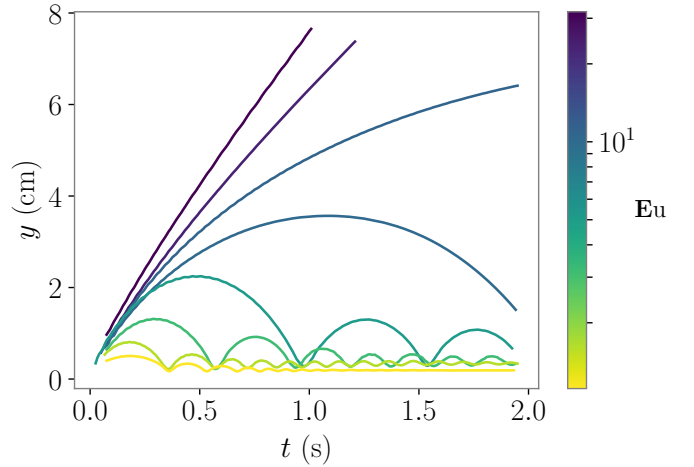


FIG. 11. Drop trajectories as a function of $\mathbb{E}u$.

Because $\mathbb{E}u \ll 1$ is not satisfied for any of the experimental drops the entire dataset is beyond the regime where the asymptotic results for short-times, given by Equation 17, are valid. However, the long-time scaled asymptotic trajectory y_c and time-of-flight t_f given by Equations 18 and 19, when redimensionalized by the short-time characteristic time $t_c = \mathbb{E}u R_d$, compare favorably to the experimental trajectory apoapses y_{max} and time-of-flight t_b as shown in Figures 14 and 15. This allows an improvement to be made to the asymptotic time-of-flight result of Equation 19 by multiplying the series by the empirical coefficient $a = 1.31$. The semi-analytic time-of-flight is then given by

$$t^* = 2.62 + 1.75\phi\mathbb{E}u + 1.05\phi^2\mathbb{E}u^2 + \mathcal{O}(\phi^3\mathbb{E}u^3). \quad (24)$$

A similar empirical coefficient $a = 1.22$ is found for

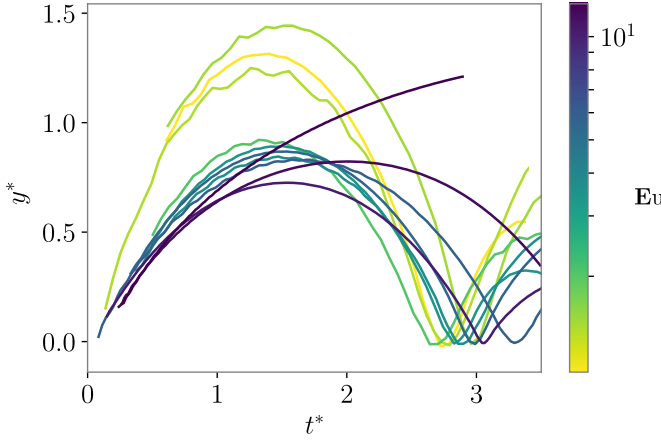


FIG. 12. Non-dimensional trajectories with the short-time scaling.

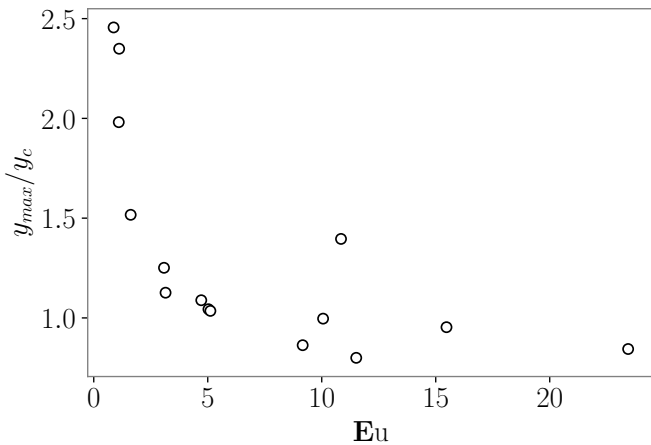


FIG. 13. Non-dimensional apoapse height y_{max}/y_c compared with Eu .

Equation 18. The relative magnitudes of the forces acting on the drops determined by the MLE numerical solutions to Equation 7 for the entire population of drop tower experiments are shown in Figure 16. Coulomb, image, and drag forces acting on the drops vary in typical magnitude between $\mathcal{O}(10^{-6})$ - $\mathcal{O}(10^{-4})$ N. We see that of the drops in the experimental dataset only the two with the largest $\text{Eu} \sim \mathcal{O}(10)$ could appropriately be said to be in the inertial electro-viscous regime. In all other cases image forces are much stronger than drag. As expected, the image forces themselves rapidly become small compared to Coulomb forces for drops with apoapses $\max(y) \gtrsim L$. The drop with largest Eu in our dataset failed to escape the electric field as the escape condition $\phi\text{Eu}/8\pi = 0.2 < 1$ was unsatisfied. Equation 24 predicts that this drop will return to the substrate after 7.4 s, a period of free-fall which is lamentably well out of reach of the Dryden Drop Tower. However, such an experiment could be performed in a drop tower facility with a longer

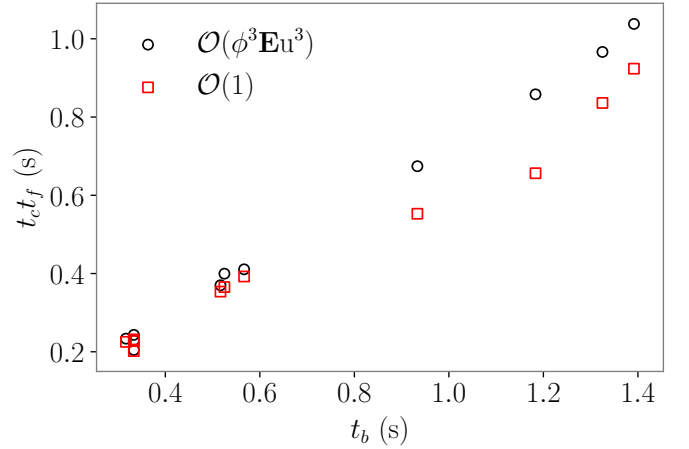


FIG. 14. Dimensional time-of-flight asymptotic estimates t_{ctf} compared with experimental time-of-flight t_b . These results compare $\mathcal{O}(1) \equiv 2t_c$ and $\mathcal{O}(\phi^3\text{Eu}^3)$ accurate variations of Equation 19.

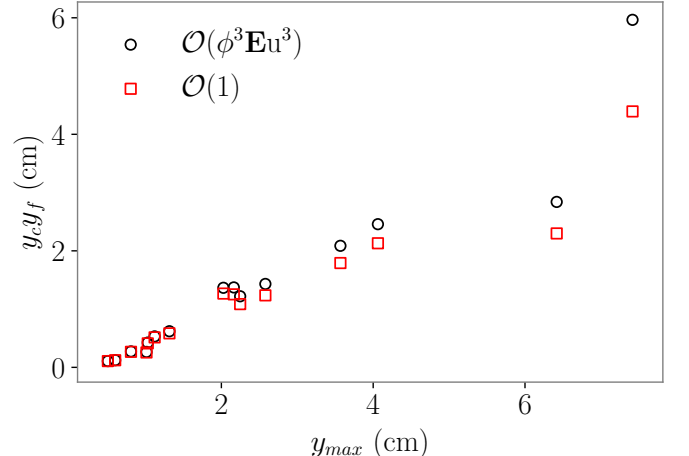


FIG. 15. Dimensional asymptotic trajectory apoapses, found from Equation 18 with $t^* = 1$ and $\mathcal{O}(1) \equiv y_c/2$, as compared to experimental apoapses y_{max} .

free fall period, aboard the ISS or on certain suborbital parabolic flights.

ACKNOWLEDGMENTS

This work was supported by NASA Cooperative Agreement NNX12A047A. We are also indebted to Andrew Greenberg for his frequent technical advice, and to Joe Shields for assistance with drop tower experiments.

¹I. M. Kirko, E. I. Dobychin, and V. I. Popov, “Phenomenon of the capillary ‘ball game’ under the condition of weightlessness,” **15**, 442.

²A. Wollman, M. Weislogel, B. Wiles, D. Pettit, and T. Snyder, “More investigations in capillary fluidics using a drop tower,” **57**, 57.

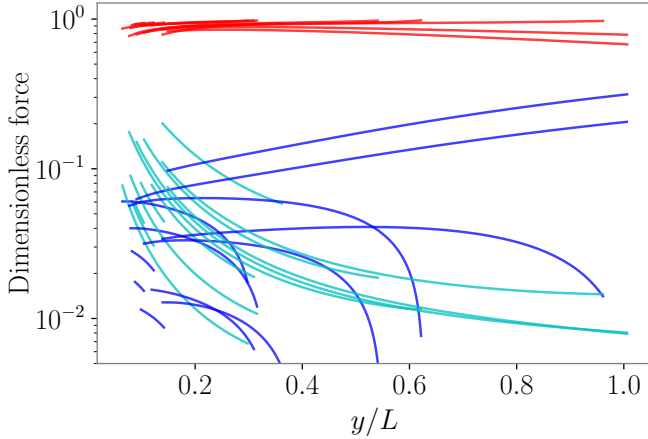


FIG. 16. Simulated forces acting on drops up to the first apoapse as determined by the MLE solutions to Equation 7 for all drops in the dataset. The (—) lines denote the Coulomb force, the (—) lines the drag force, and the (—) lines the force due to image charge respectively. The forces are scaled by the drop inertia.

- ³B. Attari, M. Weislogel, A. Wollman, Y. Chen, and T. Snyder, “Puddle jumping: Spontaneous ejection of large liquid droplets from hydrophobic surfaces during drop tower tests,” **28**, 102104.
- ⁴I. Langmuir, “Surface electrification due to the recession of aqueous solutions from hydrophobic surfaces,” **60**, 1190–1194.
- ⁵K. Yatsuzuka, Y. Mizuno, and K. Asano, “Electrification phenomena of pure water droplets dripping and sliding on a polymer surface,” **32**, 157–171.
- ⁶J. K. Beattie, “The intrinsic charge on hydrophobic microfluidic substrates,” **6**, 1409–1411.
- ⁷S. Straazdaite, J. Versluis, and H. J. Bakker, “Water orientation at hydrophobic interfaces,” **143**, 084708.
- ⁸Pettit Donald, “Flow induced charging of liquids in reduced gravity,” Proceedings, 10.1061/40177(207)75.
- ⁹D. Stevenson, “Electrostatic model applied to ISS charged water droplet experiment.”
- ¹⁰D. Choi, H. Lee, D. J. Im, I. S. Kang, G. Lim, D. S. Kim, and K. H. Kang, “Spontaneous electrical charging of droplets by conventional pipetting,” **3**, 2037.
- ¹¹D. A. Saville, “Electrohydrodynamics: The taylor-melcher leaky dielectric model,” **29**, 27–64.
- ¹²M. Hurwitz, “Electrohydrodynamic propellant management systems for cryogenic upper stages,” in *3rd Annual Meeting*, Annual Meeting (American Institute of Aeronautics and Astronautics).
- ¹³H. A. Pohl, “Some effects of nonuniform fields on dielectrics,” **29**, 1182–1188.
- ¹⁴David J. Griffiths, *Introduction to electrodynamics* (Prentice Hall).
- ¹⁵E. Schmidt, “Droplet-electro-bounce: Project files for droplet electro-bounce,” Original-date: 2017-06-06T22:20:50Z.
- ¹⁶J. Schindelin, I. Arganda-Carreras, E. Frise, V. Kaynig, M. Longair, T. Pietzsch, S. Preibisch, C. Rueden, S. Saalfeld, B. Schmid, J.-Y. Tinevez, D. J. White, V. Hartenstein, K. Eliceiri, P. Tomančák, and A. Cardona, “Fiji: an open-source platform for biological-image analysis,” **9**, 676–682.
- ¹⁷Y. Wada, H. Oguchi, M. Hara, H. Asanuma, and H. Kuwano, “Stacking electrets for electrostatic vibration energy harvesters,” in *Digest Tech. PowerMEMS 2012 Workshop*, pp. 504–507.
- ¹⁸H. Ni, R. C. Amme, and Y. Jin, “Desalination by electret technology,” **174**, 237–245.
- ¹⁹D. K. Davies, “The examination of the electrical properties of insulators by surface charge measurement,” **44**, 521.

- ²⁰T. E. Oliphant, “Python for scientific computing,” **9**, 10–20.
- ²¹J. A. Nelder and R. Mead, “A simplex method for function minimization,” **7**, 308–313.
- ²²A. Savitzky and M. J. E. Golay, “Smoothing and differentiation of data by simplified least squares procedures.” **36**, 1627–1639.
- ²³T. Takamatsu, Y. Hashimoto, M. Yamaguchi, and T. Katayama, “Theoretical and experimental studies of charged drop formation in a uniform electric field,” **14**, 178–182.